Coulomb-corrected reconstruction of ionization and recombination times in high-order harmonic generation

Mohammad Monfared* and Manfred Lein†
Leibniz University Hannover, Institute of Theoretical Physics, Appelstr. 2, 30167 Hannover, Germany
(Dated: October 7, 2025)

Accurate knowledge about electron dynamics in strong-field phenomena is crucial for understanding ultrafast processes at the attosecond scale. In this work, we improve the time-retrieval method for extracting electron ionization and return times from experimental observables in high-order harmonic generation. We address an existing approximation for the condition to maximize the harmonic intensity, and we introduce an accurate alternative equation. Furthermore, we introduce a numerical approach to incorporate Coulomb corrections into the retrieval procedure by calculating the Coulomb-induced shift of the electron velocity via integration of the Coulomb force, and the Coulomb action via integration of the Coulomb potential, both along the electron trajectories. Our refined method significantly improves the precision and reliability of the retrieved electron dynamics, establishing a robust foundation for future attosecond-scale investigations.

I. INTRODUCTION

The field of ultrafast science has made remarkable strides in probing, understanding, and controlling ultrafast quantum phenomena, with advances in laser-based techniques enabling time measurements on the attosecond scale. Among these techniques, high-order harmonic generation (HHG) has emerged as a key tool for the production of coherent extreme ultraviolet (XUV) radiation and for the study of ultrafast quantum dynamics such as electron and nuclear dynamics in gases, liquids, and solids [1–3]. HHG has been widely used for various purposes, including the generation of isolated attosecond pulses [4, 5], ultrafast spectroscopy [6], the study of tunneling dynamics [7], the characterization of molecular structure [8, 9] and molecular orbital tomography [10–12], the tracking and control of charge migration [13, 14], and the investigation of electron and lattice dynamics [15–18] in solids.

HHG is commonly described as a three-step process [19, 20], where an electron is first freed by a strong laser field, then accelerated by the field, and finally recombined with the parent ion, emitting a high-energy photon. Measurement of ionization and return times in HHG is essential to understand the underlying electron trajectories and their role in the emission of high-order harmonics. Accurate knowledge of electron trajectories provides deeper insight into attosecond phenomena and enhances the capabilities of HHG-based ultrafast spectroscopy.

In 2012, the ionization and return times in the HHG process were experimentally measured using an orthogonally polarized two-color (OTC) laser field [21]. For that purpose, a set of two equations was used as time-retrieval equations along with two experimental observables as inputs to reconstruct the ionization and return times. Within this method, a weak second-harmonic field, polarized perpendicular to the driving field, was introduced to laterally perturb the electron motion after ionization. By adjusting the phase delay between the two fields, the electron trajectory corresponding to each harmonic order can be controlled to reach two distinct cases: one phase maximizes the harmonic intensity and the other maximizes the return angle at the moment of recombination. These two optimal phases act as key input observables for the time-retrieval equations, enabling the reconstruction of both ionization and recombination times. In the pioneering experimental and theoretical studies [21, 22], the influence of the Coulomb force on the liberated electron was neglected in the time-retrieval equations. However, Coulomb effects are predicted to play a significant role in HHG [23, 24]. In particular, the analytical R-matrix (ARM) model predicts that the Coulomb interaction can shift the ionization and return times to earlier times by approximately 33–37 and 5–19 attoseconds, respectively, for a helium atom driven by an 800 nm field [23]. Despite this, theoretical studies demonstrate that ionization times can be extracted with good accuracy using higher-frequency probe fields ($\geq 4\omega$, where ω is the fundamental field frequency), even when Coulomb effects are neglected in the retrieval formalism [25]. The results of the high-frequency probing are in good agreement with the ARM theory. In fact, at high probe frequencies, the Coulomb terms in the time-retrieval equations become negligible, and the Coulomb influence is instead reflected in the optimal phases. Conversely, for lower probe field frequencies, such as 2ω with an 800 nm fundamental field, neglecting the Coulomb effect introduces an error of approximately 35 as in the retrieved ionization time [25, 26]. Recently, Yue et al. attempted to incorporate the Coulomb effect into the time-retrieval equations by considering a Coulomb-induced instantaneous kick in the electron velocity perpendicular to the fundamental field [26]. While the results from such a time retrieval showed a shift of the ionization times toward earlier times (8–20 as), they still deviated from the ARM predictions by 13–27 as, highlighting that treating the Coulomb effect as a Coulomb kick is not sufficiently accurate.

* m.monfared@yahoo.com
† lein@itp.uni-hannover.de

The extraction schemes for the ionization and return times have two main applications. First, they facilitate the measurement of these times when applied to experimental data. Second, when applied to exact numerical solutions of the time-dependent Schrödinger equation (TDSE), they allow us to check whether the analytical models are accurate.

In this study, we refine the time-retrieval equations used in the OTC method by a more accurate treatment of the Coulomb force. Unlike [26], which treated the velocity change induced by the Coulomb force as an initial kick under the assumption of constant laser electric field, our approach incorporates the Coulomb force by numerical integration over electron trajectories. The optimal phases, which serve as inputs to the time-retrieval equations, are obtained using the TDSE. Our results demonstrate reasonable agreement between the retrieved ionization times and the ARM predictions in both the low- and high-frequency regimes. Additionally, we clarify that one of the equations used in the time-retrieval method of prior studies, specifically the one related to maximizing the total harmonic intensity, is an approximation, that can lead to errors of up to 11 attoseconds in the retrieval of the ionization time for certain harmonic orders. We introduce an accurate equation to replace this approximation and obtain retrieved times in better agreement with the ARM model. These refinements improve the accuracy and robustness of the time-retrieval method, establishing a more reliable foundation for future investigations.

The article is organized as follows. Section II describes the numerical method for solving the TDSE, which is used to obtain the optimal phases as input observables, and the theoretical framework of the time-retrieval method applied to extract the ionization and recombination times. The results of our analysis are presented and discussed in Sec. III, followed by a summary of the key findings and conclusions in Sec. IV.

II. THEORETICAL MODEL

A. Time-dependent Schrödinger equation

The TDSE in the length gauge and dipole approximation is given by (atomic units are used unless otherwise stated)

$$i\frac{\partial}{\partial t}\psi(\mathbf{r},t) = \left[-\frac{1}{2}\nabla^2 + V(\mathbf{r}) + \mathbf{r}\cdot\mathbf{E}(t)\right]\psi(\mathbf{r},t). \quad (1)$$

Here, $\psi(\mathbf{r},t)$ denotes the time-dependent electron wave function at position $\mathbf{r}$. A two-dimensional soft-core potential, $V(\mathbf{r}) = -1/\sqrt{\mathbf{r}^2+a}$, with a softening parameter $a = 0.0684$ is employed to model the helium (He) atom, which has an ionization potential of $I_p = 24.6$ eV. The electric field of the OTC pulse, $\mathbf{E} = -\partial_t\mathbf{A}$, is described by the vector potential as follows

$$\mathbf{A}(t) = -\frac{E_0}{\omega}f(t)\left(\sin(\omega t)\hat{\mathbf{e}}_x + \frac{\epsilon}{n}\sin(n\omega t+\phi)\hat{\mathbf{e}}_y\right), \quad (2)$$

where $\hat{\mathbf{e}}_x$ and $\hat{\mathbf{e}}_y$ are unit vectors. The parameters E_0 and ω denote the peak field amplitude and frequency of the fundamental field. The pulse consists of three optical cycles of period $T = 2\pi/\omega$. The probe field is characterized by the frequency $n\omega$ and the field amplitude ϵE_0. The relative phase ϕ (two-color delay) controls the delay between the fundamental and probe fields. The envelope function $f(t)$ includes a one-cycle ramp-on, a one-cycle flat top, and a one-cycle ramp-off, with the ramps shaped by a $\cos^6(\omega t/4)$ function. The flat-top segment begins at $t = 0$. All simulations in this study are performed for an 800 nm fundamental laser pulse with an intensity of 4×10^{14} W/cm^2 and probe fields with various n and $\epsilon = 0.005$. The simulation box is defined on a Cartesian grid with dimensions $L_x \times L_y = 300 \times 160$ a.u., using a uniform grid spacing of 0.3 a.u. The wave function is propagated in time using a time-reversal symmetric propagator [27] with a time step of 0.02 a.u. To prevent artificial electron reflections at the boundaries, a mask function is applied. The mask function is set to 1 for $|x| \le x_0$ and $|y| \le y_0$ and gradually decreases to zero at the boundaries following a $\cos^2$-shaped function. The absorber parameters are set to $x_0 = 1.1E_0/\omega^2 = 36.2$ a.u. and $y_0 = (7/18)L_y = 62.2$ a.u. The value of x_0 is chosen such that the mask function effectively absorbs long-trajectory electrons. The TDSE simulations are carried out using the *Octopus* code [28].

Given the time-dependent wave function, the dipole acceleration can be calculated using the Ehrenfest theorem [29],

$$\mathbf{a}(t) = \langle\psi(\mathbf{r},t)|\,\partial_{\mathbf{r}}V(\mathbf{r}) + \mathbf{E}(t)\,|\psi(\mathbf{r},t)\rangle\,. \quad (3)$$

Since harmonic emission consists of contributions from several trajectories, the harmonic spectrum is not an ideal observable for retrieving emission times. Instead, we employ the Gabor transform to extract the emission data. The total Gabor intensity is defined as

$$I_G(\Omega,t) = \left|\int dt'\,\mathbf{a}(t')\,e^{-\left(t'-t\right)^2/(2\sigma^2)+i\Omega t'}\right|^2, \quad (4)$$

where Ω is the harmonic frequency and $\sigma = 1/(3\omega)$. The emission time t_e is determined as the local maximum of the total Gabor intensity I_G for each harmonic frequency Ω. For this purpose, only trajectories launched in the first half-cycle of the flat-top region of the pulse are considered. Consequently, the emission intensity at the harmonic Ω is obtained as $I_e(\Omega) = I_G(\Omega,t_e)$, and the amplitude ratio is determined by $R_e(\Omega) = \sqrt{I_{G_y}(\Omega,t_e)/I_{G_x}(\Omega,t_e)}$. Here I_{G_x} and I_{G_y} correspond to the x- and y-components of the dipole acceleration, respectively. Finally, by varying the two-color delay ϕ, one can determine the optimal phase ϕ_h that

maximizes the harmonic intensity and ϕ_a that maximizes the amplitude ratio as follows

$$\partial_\phi I_e\Big|_{\phi=\phi_h} = 0, \qquad \partial_\phi R_e\Big|_{\phi=\phi_a} = 0 \tag{5}$$

These optimal phases serve as two observables that can be used as inputs for the time-retrieval equations.

B. Strong-field approximation and quantum-orbit model

The time-retrieval equations are formulated based on the strong-field approximation (SFA) [20] and the quantum-orbit (QO) model [30]. These models do not include the Coulomb interaction. Therefore, they can serve as a reference for verifying the validity of results obtained from the time-retrieval equations in the limit where the Coulomb correction is disabled in the retrieval method, as well as for assessing the effect of the Coulomb force on the retrieved times. In the following, we briefly review the main equations of these models as employed in this study. In the SFA evaluated within the QO model, the intensity of the emitted harmonic with frequency Ω at the return time t_r is given by

$$I_s = \left| e^{-i(S-\Omega t_r)} \right|^2. \tag{6}$$

Within the SFA framework, the action S corresponds to the Volkov phase, defined as

$$S_V = \int_{t_i}^{t_r} \left[\frac{1}{2} v_x^2(t) + \frac{1}{2} v_y^2(t) + I_p \right] dt. \tag{7}$$

Here we assumed that only one trajectory is relevant.

The complex ionization and recombination times based on QO model (t_i^{QO}, t_r^{QO}) are determined by the saddle-point equations:

$$\mathbf{v}^2(t_i)/2 = -I_p, \quad \mathbf{v}^2(t_r)/2 = \Omega - I_p. \tag{8}$$

Here $\mathbf{v}(t)$ represents the electron velocity

$$\mathbf{v}(t) = \mathbf{A}(t) - \frac{1}{t_r - t_i} \int_{t_i}^{t_r} \mathbf{A}(t')dt'. \tag{9}$$

The laser-induced trajectory $\mathbf{r}_L(t) = (x_L(t), y_L(t)) = \int_{t_i}^{t} \mathbf{v}(t')dt'$ for the laser field of Eq. (2) is written as

$$x_L(t) = \frac{E_0}{\omega^2} \Bigg[\cos(\omega t) - \cos(\omega t_i) - \frac{(t-t_i)}{(t_r - t_i)} \Big(\cos(\omega t_r) - \cos(\omega t_i) \Big) \Bigg], \tag{10}$$

$$y_L(t) = \frac{\epsilon E_0}{(n\omega)^2} \Bigg[\cos(n\omega t + \phi) - \cos(\varphi_i) - \frac{(t-t_i)}{(t_r - t_i)} \Big(\cos(\varphi_r) - \cos(\varphi_i) \Big) \Bigg], \tag{11}$$

where $\varphi_i = n\omega t_i + \phi$ and $\varphi_r = n\omega t_r + \phi$.

The ionization and return times obtained from the QO model (a reference without Coulomb effects) can be compared with the results of the time-retrieval method to reveal the Coulomb-induced time shift.

C. The analytical R-matrix (ARM) model

Since we will refer to the ARM model [23] as an approach that accounts for the Coulomb interaction while predicting ionization and return times, we briefly summarize its key equations here. In this model, the total action is expressed as $S = S_V + S_C$, where S_C denotes the Coulomb-induced correction to the action, defined as

$$S_C = \int_{t_k}^{t_f} U_C(\mathbf{r}_L(t))\, dt. \tag{12}$$

Here, $\mathbf{r}_L(t)$ represents the laser-induced Coulomb-free trajectory defined by Eqs. (10) and (11). The integration interval is defined with the lower limit $t_k = t_i - i/(2I_p)$, while the upper limit t_f is obtained by enforcing the return condition

$$\sqrt{\mathbf{r}_L(t_f)^2} = \frac{\exp\left[2(0.5772 - \xi)\right]}{2v_r}, \tag{13}$$

where

$$\xi = \sum_{p=1}^{\infty} \left[\frac{1}{p} - v_r \arctan\left(\frac{1}{v_r p} \right) \right], \tag{14}$$

and the return velocity is given by $v_r = \sqrt{2(\Omega - I_p)}$.

Assuming that the Coulomb-induced action S_C is small compared to S_V, one can approximately solve the Coulomb-corrected saddle-point equations. This yields the first-order corrections to the ionization and return times [23]:

$$\Delta t_i^{\mathrm{ARM}} = -\frac{\partial S_c}{\partial I_p} - \frac{\partial S_c}{\partial \Omega}, \qquad \Delta t_r^{\mathrm{ARM}} = -\frac{\partial S_c}{\partial \Omega}, \tag{15}$$

where the partial derivatives act on those parts of S_c that depend on I_p and Ω through the times t_i and t_r. Therefore, ARM times are obtained as

$$t_i^{\mathrm{ARM}} = t_i^{\mathrm{QO}} + \Delta t_i^{\mathrm{ARM}}, \qquad t_r^{\mathrm{ARM}} = t_r^{\mathrm{QO}} + \Delta t_r^{\mathrm{ARM}}. \tag{16}$$

D. Time-retrieval equations

The time-retrieval equations proposed and used in prior studies [21, 22, 26] read

$$\mathrm{Re}\, v_{\mathrm{y0}}\Big|_{\phi=\phi_h} = 0, \quad \partial_\phi R\Big|_{\phi=\phi_a} = 0. \tag{17}$$

Here, v_{y0} represents the initial lateral velocity of the electron at the ionization moment t_i. R is the amplitude ratio

defined as $R = |v_y(t_r)/v_x(t_r)|$, where $v_x(t_r)$ and $v_y(t_r)$ denote the return velocities along the x-axis and y-axis, respectively, evaluated at the return time t_r. For v_{y0} and R, analytical expressions are used that depend on the two-color delay ϕ and the times t_i and t_r. Thus, from the knowledge of the measurable quantities ϕ_h and ϕ_a and using Eq. (17), the times t_i and t_r can be obtained. The initial lateral velocity and the amplitude ratio, including Coulomb corrections, can be expressed as follows:

$$v_{y0} = -\frac{\epsilon E_0}{n\omega}\left[\sin(\varphi_i) + \frac{\cos(\varphi_r) - \cos(\varphi_i)}{n\omega(t_r - t_i)}\right] - \frac{\Delta y^C(t_i, t_r)}{t_r - t_i}, \tag{18}$$

$$R = \frac{1}{\sqrt{2(\Omega - I_p)}}\left| -\frac{\epsilon E_0}{n\omega}\left[\sin(\varphi_r) + \frac{\cos(\varphi_r) - \cos(\varphi_i)}{n\omega(t_r - t_i)}\right] + \Delta v_y^C(t_i, t_r) - \frac{\Delta y^C(t_i, t_r)}{(t_r - t_i)}\right|. \tag{19}$$

Here, Δv_y^C and Δy^C represent the velocity change and displacement of the electron along the y-axis, respectively, induced by the Coulomb force during the excursion time (from $\mathrm{Re}\, t_i$ to $\mathrm{Re}\, t_r$). Since t_i and t_r in the above equations are generally complex values, additional assumptions are required for their imaginary parts. For the imaginary part of the ionization time, a suitable choice is to adopt the Keldysh tunneling time defined as $\mathrm{Im}\, t_i = \tau_K = \sqrt{2I_p}/|E_x(\mathrm{Re}\, t_i)|$ [25]. The simplest assumption for the imaginary part of the return time is $\mathrm{Im}\, t_r = 0$. Although this assumption may be effective to some extent [26], our analysis of the new implementation of Coulomb corrections in the time-retrieval equations (presented in the subsequent section) indicates that it leaves room for improvement. A more accurate alternative, employed throughout this work, is to adopt the value of $\mathrm{Im}\, t_r$ from the ARM times Eq. (16).

If the Coulomb force effect is approximated as a short kick induced at $t = \mathrm{Re}\, t_i$, as used in Refs. [26, 31, 32], then the Coulomb terms in Eqs. (18) and (19) result in

$$\Delta v_y^C(t_i, t_r) = u_0^C = \frac{\epsilon\, \pi E_0 \cos\left(n\omega\, \mathrm{Re}\, t_i + \phi\right)}{(2I_p)^{3/2}}, \tag{20}$$

$$\Delta y^C(t_i, t_r) = (t_r - \mathrm{Re}\, t_i) u_0^C. \tag{21}$$

By substituting Eqs. (20) and (21) into Eqs. (18) and (19), we obtain the same retrieval equations used in Ref. [26] (Eqs. (11) and (14) in [26]). As demonstrated in [26], this approximation results in a shift of the ionization time to earlier times at lower probe frequencies; however, the retrieved times remain significantly different from the prediction of the ARM model.

To achieve a more accurate Coulomb correction for the time-retrieval equations, we propose an alternative approach. The Coulomb-induced velocity change can be calculated via Coulomb force integration as follows

$$\Delta v_y^C(t_i, t) = \int_{t_1}^{t} F_y^C(t')\, dt', \tag{22}$$

where t_1 represents the starting time of electron excursion, and the y-component of the Coulomb force is given by

$$F_y^C(t) = -\frac{\partial V(\mathbf{r})}{\partial y} = -\frac{y_L(t)}{\left(x_L^2(t) + y_L^2(t)\right)^{3/2}}. \tag{23}$$

To obtain the time-dependent Coulomb force, we require the electron trajectories. Here, we use the Coulomb-free laser-induced trajectories as an approximation (Eqs. (10) and (11)). By evaluating Eq. (22) at the end of the electron excursion, $t = t_2$, we obtain the Coulomb-induced change in velocity accumulated over the entire excursion as

$$\Delta v_y^C(t_i, t_r) = \int_{t_1}^{t_2} F_y^C(t')\, dt'. \tag{24}$$

Finally, the electron displacement along the y-axis for the entire excursion interval $[t_1,\ t_2]$ is obtained as

$$\Delta y^C(t_i, t_r) = \int_{t_1}^{t_2} \Delta v_y^C(t_i, t')\, dt'. \tag{25}$$

Two possible choices for the integral limits t_1 and t_2 in the above equations are $[\mathrm{Re}\, t_i,\ \mathrm{Re}\, t_r]$ and $[t_k,\ t_f]$, which are discussed in Section II F.

E. Modified time-retrieval equations

The first relation in the time-retrieval equations (Eq. (17)) is derived by maximizing the tunneling rate with respect to the two-color delay ϕ [21]. In this approach, it is assumed that the dependence of the tunneling rate on ϕ occurs through the real-valued initial transverse velocity as $\Gamma \propto \exp\left(-(\mathrm{Re}\, v_{y0})^2 \tau_K/2\right)$. In fact, this equation arises from a tunneling picture. To derive a more accurate equation for this purpose, one can begin by maximizing the harmonic intensity $\partial_\phi I_s = 0$ based on the SFA. Using Eq. (6), this maximization simplifies to $\partial_\phi[\mathrm{Im}\, S] = 0$. Here, we use a small scaling factor ϵ to ensure that t_r remains independent of ϕ. Therefore, we propose the following modified time-retrieval equations for the OTC scheme:

$$\partial_\phi[\mathrm{Im}\, S]\Big|_{\phi=\phi_h} = 0, \quad \partial_\phi R\Big|_{\phi=\phi_a} = 0, \tag{26}$$

where R is the same quantity as defined in Eq. (19). In the Coulomb-free approximation, we have $S = S_V$. To incorporate the Coulomb effect, one can use $S = S_V + S_C$, where the Coulomb correction S_C is given by the same expression as used in the ARM model, Eq. (12).

Table I. Overview of time-retrieval methods, assumptions, and equations adopted in this study.

Method	Abbreviation	Equations	Assumptions	
Time-retrieval with Coulomb corrections as an initial kick [26]	TRC-kick	17-21	$\mathrm{Im}\, t_i = \tau_K$,	$\mathrm{Im}\, t_r = 0$
Time-retrieval with Coulomb corrections via Coulomb force integration	TRC-integration	17-19, 22-25	$\mathrm{Im}\, t_i = \mathrm{Im}\, t_i^{\mathrm{ARM}}$,	$\mathrm{Im}\, t_r = \mathrm{Im}\, t_r^{\mathrm{ARM}}$
Modified time-retrieval with Coulomb corrections via the Coulomb action	MTRC-integration	26, 12, 19, 22-25	$\mathrm{Im}\, t_i = \mathrm{Im}\, t_i^{\mathrm{ARM}}$,	$\mathrm{Im}\, t_r = \mathrm{Im}\, t_r^{\mathrm{ARM}}$

F. Overview of Time-Retrieval Methods and Assumptions Adopted in This Study

In this study, we consider three different time-retrieval methods for extracting ionization and return times, based on the equations introduced in the previous subsections. We provide further details on the assumptions underlying these methods, along with the abbreviations used, in Table I. For the TRC-integration method, the integration limits $t_1 = \mathrm{Re}\, t_i$ and $t_2 = \mathrm{Re}\, t_r$ are chosen, as they yield more accurate retrieved times than the complex integration limits. In the MTRC-integration method, the limits $t_1 = t_k$ and $t_2 = t_f$ are selected to maintain consistency with the integration limits used in the Coulomb action S_C (Eq. 12). It should be noted that $\mathrm{Re}\, t_i$ and $\mathrm{Re}\, t_r$ in the integral bounds (appearing in t_1, t_2, t_k, and t_f) are treated as unknown variables in the time-retrieval process, rather than being fixed known values (such as those from the QO or ARM models). In this study, all retrieved times are calculated by inserting the optimal phases extracted from the TDSE into the time-retrieval equations. The abbreviations in Table I are used consistently throughout the results presented in this work.

III. RESULTS

A. Retrieved times with Coulomb corrections as an initial kick

We begin by presenting results obtained using the time-retrieval method that incorporates Coulomb corrections by modeling the Coulomb interaction as an initial kick to the electron velocity (TRC-kick). We compare the retrieved times with those predicted by the QO and ARM models, which exclude and include the Coulomb effect, respectively, see Fig. 1(a). The method and assumptions employed in TRC-kick are exactly the same as those used in [26]. For an OTC scheme with an $\omega - 2\omega$ configuration (blue dashed curves), the retrieved ionization time obtained by TRC-kick shows a shift toward earlier times (about 10 attoseconds at intermediate harmonics) compared to the QO model. Although this shift toward earlier times is expected, it still exhibits considerable deviation from the ARM results. The retrieved return time exhibits a similar shift toward earlier times, showing good agreement for the intermediate harmonics but slightly underestimating the shift for lower harmonics and overestimating it for higher harmonics compared to the ARM result.

For the $\omega - 4\omega$ configuration in Fig. 1(a), the retrieved

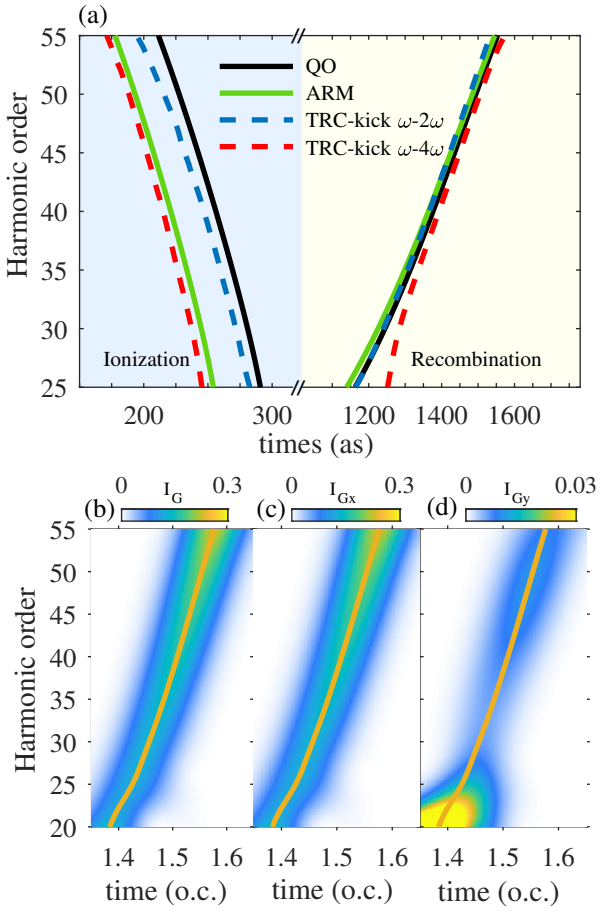

Figure 1. (a) Retrieved ionization and return times ($\mathrm{Re}\, t_i$, $\mathrm{Re}\, t_r$) from TDSE results for an OTC scheme with $\omega - 2\omega$ and $\omega - 4\omega$ fields. The black solid lines indicate the real parts of the times calculated using the Coulomb-free QO model, while the green solid lines represent the times from the ARM model. Retrieved times obtained from the original time-retrieval method with Coulomb corrections modeled as an initial kick (TRC-kick) are depicted by blue ($\omega - 2\omega$) and red ($\omega - 4\omega$) dashed curves. The temporal regions corresponding to ionization and recombination are highlighted with light-blue and light-yellow shaded areas, respectively. (b)-(d) The Gabor time–frequency profile of the total harmonic emission I_G, the x-component I_{G_x}, and the y-component I_{G_y} for the probe frequency 4ω. The yellow solid curves represents the emission times extracted from the maxima of the total Gabor intensity in (b), for each harmonic order. Calculations are performed for an OTC field with a fundamental wavelength of 800 nm and a peak intensity of 4×10^{14} W/cm^2. The probe field has the scaling factor $\epsilon = 0.005$. For panels (b)-(d), the two-color delay is set to $\phi = 0$.

ionization times are in a better agreement with the prediction of the ARM model, with a deviation of 5-9 attoseconds. Indeed, for an OTC laser scheme with a high-frequency probe field, the Coulomb interaction significantly manifests in the optimal phases [25], while the Coulomb-related terms in the time-retrieval equations become negligible compared to the laser-driven terms. Consequently, the ionization time can be retrieved with reasonable accuracy for higher probe frequencies even without explicitly including Coulomb corrections in the time-retrieval equations [25]. The right panel of Fig. 1(a) reveals that the retrieved return times for the intermediate and high harmonics match closely with the QO model, with a shift of approximately 12-30 attoseconds to later times, while the ARM model predicts earlier times. The return times for low harmonics significantly deviate from both QO and ARM models. This discrepancy may arise from uncertainties in accurately determining the optimal phases ϕ_a in the H25–H30 region, due to the dip-like structure observed in the y-component of the Gabor transform (I_{G_y}), as illustrated in Fig. 1(d). This dip could result from the merging of two branches visible in the Gabor transform I_{G_y}. While resolving the influence of intensity minima on optimal phases is beyond the scope of this study, our approach remains applicable to regions of the plateau that are unaffected by these minima. The yellow solid curve in Fig. 1 represents the emission times extracted from the maxima of the total Gabor intensity $I_G = I_{G_x} + I_{G_y}$ (Fig. 1(b)) for each harmonic order.

B. Retrieved times with Coulomb corrections via Coulomb force/potential integration

Here, we present our results for the time-retrieval methods with Coulomb corrections (TRC-integration and MTRC-integration), in which the Coulomb effects are incorporated through integration of the Coulomb force or potential along the electron trajectories. Figure 2(a) compares the retrieved ionization and return times obtained from the TRC-integration method with the reference QO and ARM times, for both ω-2ω and ω-4ω configurations. The TRC-integration method shows a slight improvement in retrieving the ionization time for the ω–2ω case, exhibiting a larger shift toward earlier times, approximately 17 attoseconds. The retrieved ionization times for the ω–4ω configuration show a deviation of 6-10 attoseconds compared to the ARM prediction. Fig. 2(b) shows the retrieved ionization and return times obtained using the MTRC-integration method. As can be seen, shifts of the retrieved ionization times for the ω–2ω case remain underestimated: the shift is approximately 16 attoseconds toward earlier times compared to the QO times. In contrast, for the ω–4ω case, the retrieved ionization times show perfect agreement with the ARM prediction.

The retrieved return times from TRC-integration and

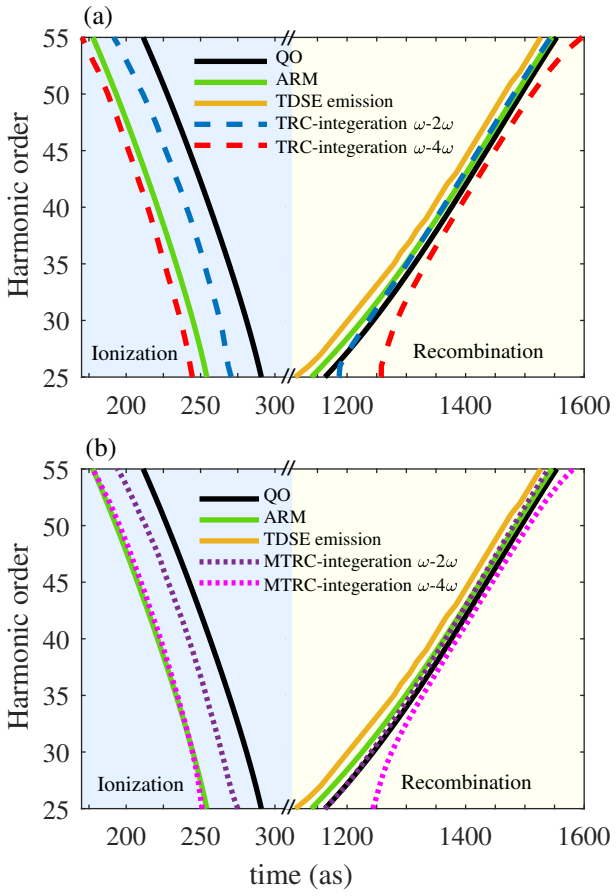

Figure 2. Ionization and return times retrieved from TDSE results using (a) TRC-integration and (b) MTRC-integration methods. The black solid lines indicate the real parts of the times calculated using the Coulomb-free QO model, and the green solid lines represent the times from the ARM model. The TDSE emission times (yellow solid curve) are extracted from the maxima of the total Gabor time–frequency profile.

MTRC-integration methods exhibit the same trend as observed with the Coulomb kick approach, with a slight improvement in agreement with the ARM prediction at higher harmonic orders. In Fig. 2, we also show a comparison with the TDSE emission times (yellow curve). There is a discrepancy with the ARM/retrieved times, which may arise from the absence of transition-dipole effects in the latter methods.

Finally, we investigate the accuracy of the retrieved times obtained using the proposed methods in this work (the TRC-integration and MTRC-integration methods) across various probe field frequencies. Fig. 3(a) and (b) shows the retrieved ionization time as a function of probe field frequency for harmonic orders H45 and H55. As can be seen, the retrieved ionization times exhibit better agreement with the ARM prediction at higher probe frequencies, particularly for the MTRC-integration method. For lower probe frequency, the deviation from the ARM model is substantial, reaching a

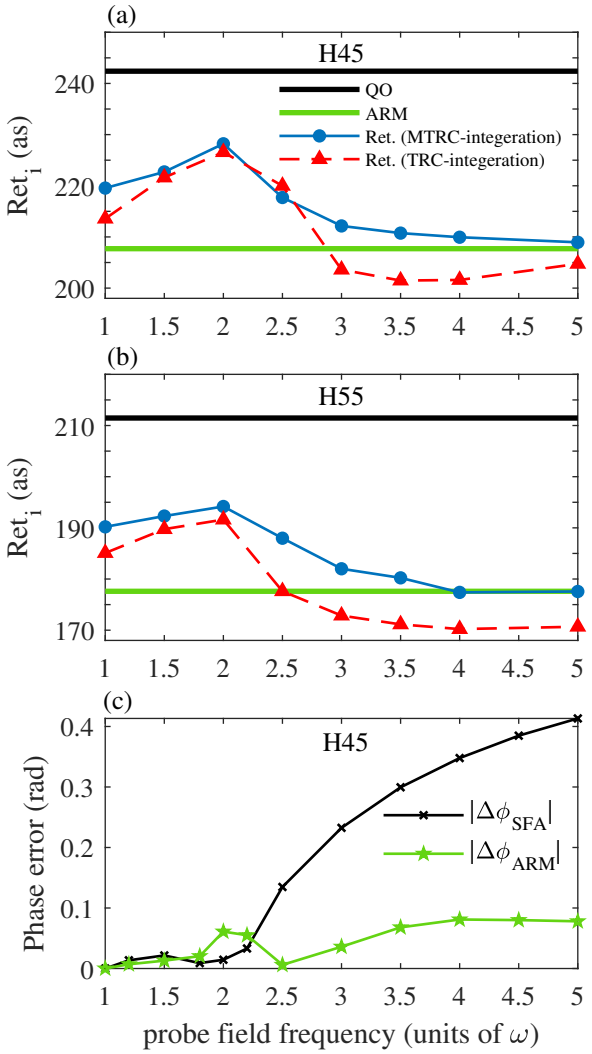

Figure 3. Ionization times as a function of the probe frequency for harmonic orders (a) H45 and (b) H55. The retrieved times shown as blue (red) lines with solid circles (triangles) are calculated using the MTRC(TRC)-integration method. The black and green solid lines indicate the QO and ARM reference times, respectively. (c) The errors in optimal phases obtained from the SFA and ARM models versus the probe frequency. The errors are defined with respect to the TDSE optimal phases, which correspond to the maxima of the total harmonic intensity.

maximum near the probe frequency 2ω. For probe frequencies below 2ω, the deviation gradually decreases. The maximum of the errors near 2ω can be attributed to the limited accuracy of Coulomb action or Coulomb force integrations around this frequency. Figure 3(c) shows the errors in the optimal phases obtained from the SFA and ARM models, with $\Delta\phi_{\rm SFA} = \phi_{\rm TDSE} - \phi_{\rm SFA}$ and $\Delta\phi_{\rm ARM} = \phi_{\rm TDSE} - \phi_{\rm ARM}$. Here, $\phi_{\rm TDSE}$, $\phi_{\rm SFA}$, and $\phi_{\rm ARM}$ represent the optimal phases for maximizing the total harmonic intensity, obtained from TDSE, SFA, and ARM, respectively. The ARM optimal phases are obtained by evaluating the action using ARM times computed for the OTC field. The ARM phase error is expected to be smaller than the SFA phase error due to the inclusion of Coulomb corrections in the ARM model. Indeed, the results reveal a reduction of the phase error at both high and low probe frequencies compared to the SFA. However, an increased error is observed near 2ω. This counterintuitive finding may be related to the fact that the ARM model considers only first-order Coulomb corrections by construction.

IV. CONCLUSIONS

In this work, we have introduced two refinements to the time-retrieval equations for reconstructing ionization and return times from observables in an OTC scheme, applicable to both experiments and simulations. First, we developed an improved approach to incorporate Coulomb corrections into the time-retrieval method. Rather than modeling the Coulomb effect as an instantaneous initial momentum kick [26], we account for Coulomb effects by integrating the Coulomb force along the electron trajectories. This approach captures Coulomb-induced time shifts in the ionization time with greater accuracy and yields improved agreement with the ARM predictions. Second, we propose a revised equation for maximizing the harmonic intensity as a function of the two-color delay. The results of this refinement demonstrate a notably reduced deviation between the retrieved times and the ARM predictions at higher probe frequencies. However, even with both refinements, the retrieval method captures only about half of the time shift predicted by the ARM model when using lower probe frequencies, especially near the experimentally convenient frequency 2ω. Overall, these refinements offer a more precise framework for attosecond-scale measurements and provide deeper insights into strong-field phenomena.

[1] J. Li, J. Lu, A. Chew, S. Han, J. Li, Y. Wu, H. Wang, S. Ghimire, and Z. Chang, Attosecond science based on high harmonic generation from gases and solids, Nature Communications **11**, 2748 (2020).
[2] R. Weissenbilder, S. Carlström, L. Rego, C. Guo, C. Heyl, P. Smorenburg, E. Constant, C. Arnold, and A. L'huillier, How to optimize high-order harmonic generation in gases, Nature Reviews Physics **4**, 713 (2022).
[3] D. Villeneuve, Attosecond science, Contemporary Physics **59**, 47 (2018).
[4] J. Li, X. Ren, Y. Yin, K. Zhao, A. Chew, Y. Cheng, E. Cunningham, Y. Wang, S. Hu, Y. Wu, *et al.*, 53-

attosecond x-ray pulses reach the carbon K-edge, Nature Communications **8**, 186 (2017).
[5] T. Gaumnitz, A. Jain, Y. Pertot, M. Huppert, I. Jordan, F. Ardana-Lamas, and H. J. Wörner, Streaking of 43-attosecond soft-x-ray pulses generated by a passively CEP-stable mid-infrared driver, Optics Express **25**, 27506 (2017).
[6] R. Borrego-Varillas, M. Lucchini, and M. Nisoli, Attosecond spectroscopy for the investigation of ultrafast dynamics in atomic, molecular and solid-state physics, Reports on Progress in Physics **85**, 066401 (2022).
[7] O. Kneller, D. Azoury, Y. Federman, M. Krueger, A. J. Uzan, G. Orenstein, B. D. Bruner, O. Smirnova, S. Patchkovskii, M. Ivanov, *et al.*, A look under the tunnelling barrier via attosecond-gated interferometry, Nature Photonics **16**, 304 (2022).
[8] L. He, C. Yuen, Y. He, S. Sun, E. Goetz, A.-T. Le, Y. Deng, C. Xu, P. Lan, P. Lu, *et al.*, Ultrafast picometer-resolved molecular structure imaging by laser-induced high-order harmonics, Physical Review Letters **133**, 023201 (2024).
[9] P. M. Kraus, A. Rupenyan, and H. J. Wörner, High-harmonic spectroscopy of oriented OCS molecules: emission of even and odd harmonics, Physical Review Letters **109**, 233903 (2012).
[10] J. Itatani, J. Levesque, D. Zeidler, H. Niikura, H. Pépin, J.-C. Kieffer, P. B. Corkum, and D. M. Villeneuve, Tomographic imaging of molecular orbitals, Nature **432**, 867 (2004).
[11] C. Vozzi, M. Negro, F. Calegari, G. Sansone, M. Nisoli, S. De Silvestri, and S. Stagira, Generalized molecular orbital tomography, Nature Physics **7**, 822 (2011).
[12] Z. Ren, Y. Yang, Y. Zhu, X. Zan, J. Zhao, and Z. Zhao, Three-dimensional tomographic imaging of co molecular orbitals reveals multi-electron effects, Journal of Physics B: Atomic, Molecular and Optical Physics **54**, 185601 (2021).
[13] L. He, S. Sun, P. Lan, Y. He, B. Wang, P. Wang, X. Zhu, L. Li, W. Cao, P. Lu, *et al.*, Filming movies of attosecond charge migration in single molecules with high harmonic spectroscopy, Nature Communications **13**, 4595 (2022).
[14] P. M. Kraus, B. Mignolet, D. Baykusheva, A. Rupenyan, L. Horný, Éric F. Penka, G. Grassi, O. I. Tolstikhin, J. Schneider, F. Jensen, L. B. Madsen, A. D. Bandrauk, and H. J. Wörner, Measurement and laser control of attosecond charge migration in ionized iodoacetylene, Science **350**, 790 (2015).
[15] S. M. Cavaletto, K. M. Kowalczyk, F. O. Navarrete, and J. Rivera-Dean, The attoscience of strong-field-driven solids, Nature Reviews Physics , 1 (2024).
[16] C. Heide, Y. Kobayashi, S. R. U. Haque, and S. Ghimire, Ultrafast high-harmonic spectroscopy of solids, Nature Physics **20**, 1546 (2024).
[17] E. Goulielmakis and T. Brabec, High harmonic generation in condensed matter, Nature Photonics **16**, 411 (2022).
[18] J. Zhang, Z. Wang, F. Lengers, D. Wigger, D. E. Reiter, T. Kuhn, H. J. Wörner, and T. T. Luu, High-harmonic spectroscopy probes lattice dynamics, Nature Photonics **18**, 792 (2024).
[19] P. B. Corkum, Plasma perspective on strong field multiphoton ionization, Physical Review Letters **71**, 1994 (1993).
[20] M. Lewenstein, P. Balcou, M. Y. Ivanov, A. L'huillier, and P. B. Corkum, Theory of high-harmonic generation by low-frequency laser fields, Physical Review A **49**, 2117 (1994).
[21] D. Shafir, H. Soifer, B. D. Bruner, M. Dagan, Y. Mairesse, S. Patchkovskii, M. Y. Ivanov, O. Smirnova, and N. Dudovich, Resolving the time when an electron exits a tunnelling barrier, Nature **485**, 343 (2012).
[22] J. Zhao and M. Lein, Determination of ionization and tunneling times in high-order harmonic generation, Physical Review Letters **111**, 043901 (2013).
[23] L. Torlina and O. Smirnova, Coulomb time delays in high harmonic generation, New Journal of Physics **19**, 023012 (2017).
[24] S. V. Popruzhenko, Coulomb phase in high harmonic generation, Journal of Physics B: Atomic, Molecular and Optical Physics **51**, 144006 (2018).
[25] S. Yue, S. Xue, H. Du, and M. Lein, Revealing coulomb time shifts in high-order harmonic generation by frequency-dependent streaking, Physical Review A **105**, L041103 (2022).
[26] S. Yue, J. Liu, S. Xue, H. Du, and M. Lein, Observing the coulomb shifts of ionization times in high-order harmonic generation, Physical Review A **107**, 063102 (2023), Erratum: Physical Review A 111, 039902 (2025), doi:10.1103/PhysRevA.111.039902.
[27] A. Castro, M. A. Marques, and A. Rubio, Propagators for the time-dependent Kohn-Sham equations, The Journal of Chemical Physics **121**, 3425 (2004).
[28] N. Tancogne-Dejean, M. J. Oliveira, X. Andrade, H. Appel, C. H. Borca, G. Le Breton, F. Buchholz, A. Castro, S. Corni, A. A. Correa, *et al.*, Octopus, a computational framework for exploring light-driven phenomena and quantum dynamics in extended and finite systems, The Journal of Chemical Physics **152**, 124119 (2020).
[29] K. Burnett, V. Reed, J. Cooper, and P. Knight, Calculation of the background emitted during high-harmonic generation, Physical Review A **45**, 3347 (1992).
[30] P. Salieres, B. Carré, L. Le Déroff, F. Grasbon, G. Paulus, H. Walther, R. Kopold, W. Becker, D. Milosevic, A. Sanpera, *et al.*, Feynman's path-integral approach for intense-laser-atom interactions, Science **292**, 902 (2001).
[31] S. Goreslavski, G. Paulus, S. Popruzhenko, and N. Shvetsov-Shilovski, Coulomb asymmetry in above-threshold ionization, Physical Review Letters **93**, 233002 (2004).
[32] N. Shvetsov-Shilovski, S. Goreslavski, S. Popruzhenko, and W. Becker, Capture into Rydberg states and momentum distributions of ionized electrons, Laser Physics **19**, 1550 (2009).